Journal of Materials Chemistry C

ROYAL SOCIETY OF CHEMISTRY

PAPER

View Article Online
View Journal | View Issue

Cite this: J. Mater. Chem. C, 2025, 13, 273

Revisiting the excited state proton transfer dynamics in *N*-oxide-based fluorophores: a keto–enol/enolate interplay to detect trace water in organic solvents†

Savita, Adarash Kumar Shukla and Anupam Bhattacharya *

This work highlights the unique proton transfer ability observed in cyanoquinoxaline *N*-oxide-based fluorophores. A fluorophore HCQ was synthesized for this purpose, and a detailed study of its photophysical characteristics was undertaken. Preliminary structural characterization by NMR and single crystal XRD techniques indicated the possibility of a ground-state proton transfer (GSPT) reaction in the molecule. The absorbance and fluorescence spectroscopic studies further confirmed its sensitivity to the solvent environment and the possibility of the existence of three species enol (E)/enolate (RO^-)/keto (K), with the predominance for a particular form based on the polarity of the solvent. Measurement of the fluorescence lifetime of the molecule allowed us to establish the role of protic solvents in the deprotonation of HCQ. In addition, the involvement of water in crystal packing and the significantly reduced lifetime of the molecule in water indicated the involvement of GSIPT and ESIPT processes. Based on the unique response of the molecule in the aqueous medium, its application for water detection in organic solvents was explored. HCQ demonstrated a water-induced fluorescence switch from its enol (E) form to the deprotonated (RO^-)/keto (K) form, showcasing distinct spectral responses across various solvents with LOQ values in the range of 0.09–0.9%. The results were finally validated through Karl Fischer titration, showing similar outcomes.

Received 25th June 2024,
Accepted 19th October 2024

DOI: 10.1039/d4tc02651a

rsc.li/materials-c

Introduction

Excited state proton transfer dynamics, from salicylic acid to benzothiazoles and flavones, have been well explored and utilized for various applications.[1] *N*-Oxide-based systems, on the other hand, are versatile tools in various fields, including medicinal chemistry, where their utility as reactive intermediates and pharmaceutical agents is well recognized.[2–6] The investigations on the excited state dynamics of these systems, particularly as fluorophores, remain largely unexplored. Given their significant biological activity, understanding their optical properties becomes crucial, as it can expand their applications as probes for bioimaging and material applications.[7] The *N*-oxide group in these compounds acts as the proton acceptor site, whereas the presence of electron-donating/accepting groups on the scaffold increases the scope for spectral tuning (Scheme 1).[8] In addition, introducing an amino/hydroxyl group in the neighbouring sites allows the possibility of intra/intermolecular proton transfer processes.

The excited state intramolecular proton transfer (ESIPT) is one of the most well-recognized mechanisms observed in the photochemical processes. ESIPT materials typically use π-delocalization/intramolecular hydrogen bonding for proton transfer.[9] Different molecules with the abovementioned features are known to utilize the ESIPT route. However, research on proton transfer materials based on O/N–H···O^-–N^+ type

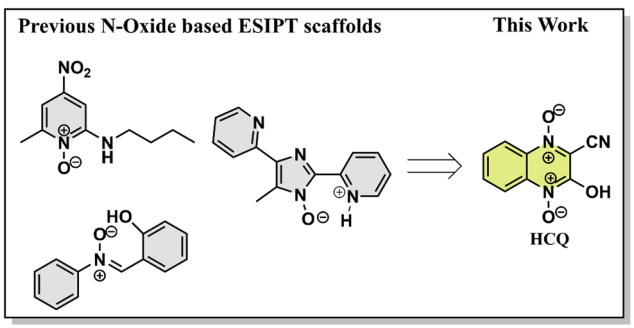

Scheme 1 Structures of known fluorophores with the O/N–H···O^-–N^+ ESIPT site and fluorophore studied in this work.

Department of Chemistry, Birla Institute of Technology and Science-Pilani (Hyderabad Campus), Hyderabad-500078, India.
E-mail: anupam@hyderabad.bits-pilani.ac.in; Tel: +91-40-66303522

† Electronic supplementary information (ESI) available. CCDC 2270859. For ESI and crystallographic data in CIF or other electronic format see DOI: https://doi.org/10.1039/d4tc02651a

intramolecular hydrogen bonding is limited. One of the initial reports on these systems was by Poór *et al.*, who investigated the impact of an amino substituent in the *ortho* position on the excited-state dynamics. The molecule studied was 2-butylamino-6-methyl-4-nitropyridine *N*-oxide (2B6M), where intramolecular charge transfer triggered an intramolecular proton transfer.[10] The same research group later determined the hydrogen bonding pattern in 2B6M using crystal structure analysis, and experimental/theoretical studies confirmed ESIPT in polar solvents like acetonitrile.[11] Later, de Klerk *et al.* studied the same system and explored its behavior in nonpolar solvents. The study concluded that a monomeric ground state species dominates in the liquid state, emitting through two distinct pathways *via* internal proton-transfer processes from the normal and tautomeric excited states.[12] A separate study on 2B6M revealed its unique fluorescence behavior in nonpolar solvents, where ratios and quantum yield of normal and tautomeric forms varied with excitation wavelength, challenging the Kasha–Vavilov rule. Transient absorption spectroscopy and fluorescence decay were used to identify multiple decay pathways, along with a detailed analysis of the impact of solvent polarity.[13,14] The studies concluded that it might not be the S_2 state but rather the high-energy vibrational mode of the S_1 state that was involved. However, despite the abovementioned reports, a precise proton transfer mechanism remains elusive.[15]

Another series of rare ESIPT emitters are based on the 1-hydroxy-1*H*-imidazole scaffold. Shekhovtsov and coworkers demonstrated anti-Kasha ($S_2 \rightarrow S_0$) emission behavior on (5-(4-fluorophenyl)-1-hydroxy-4-methyl-1*H*-imidazol-2-yl)(phenyl)methanone (HL).[16] The study focussed on HL's proton transfer abilities, featuring an intramolecular N–O–H···N hydrogen bonding. The authors also demonstrated that the emission was excitation wavelength-dependent in CH_3CN and the solid state, while in EtOH, the emission was relatively blue-shifted.[17,18] The role of the π-conjugated quinoline-2-yl group in proton transfer processes and the influence of Zn^{2+} on the photochemistry and photophysics of an HL analog were also explored in another study.[19] The same research group also explored the ESIPT feature of the HL core by increasing the number of donor N atoms and extending the π-system.[20,21] Another compound that follows the ESIPT mechanism is α-(2-hydroxyphenyl)-*N*-phenylnitrone (Nit–OH). In this system, excited-state intramolecular proton transfer (ESIPT), twisted intramolecular charge transfer (TICT), and aggregation-induced emission in Nit–OH were investigated, which provide insights into the complex photophysical behavior of the molecule.[22]

Despite the wide scope for utility, there remains a gap in understanding the photophysics of these compounds. The current research work attempted to address this gap by investigating the optical characteristics of a substituted cyanoquinoxaline *N*-oxide (HCQ). The main objective of this study was to carry out a detailed study of its absorption and fluorescence processes across various solvent environments. Additionally, the enol/enolate/keto tautomerization phenomenon possible in the molecule was also studied by correlating fluorescence spectral features with the time-correlated single photon counting (TCSPC) data. Based on the photophysical studies, we also explored the application of HCQ.

Experimental section

Instruments

Nuclear magnetic resonance (NMR) spectroscopy: Both proton ^1H and ^{13}C NMR spectra were obtained using a Bruker AV NEO (400 MHz). HRMS data were collected using an Agilent 6546 LC/Q-TOF (Model AJS-ESI). Absorption and emission spectra were recorded using a UV-visible spectrophotometer Jasco V-650 and Horiba, Fl-3C, respectively. The time-correlated single-photon counting (TCSPC) technique was employed to determine time-resolved fluorescence measurements using Horiba DeltaFlex-01, Nano LEDs 405 L, 440 L, 510 L. Crystal data were procured using a single crystal XRD Rigaku Oxford XTALAB. The percentage of water in samples was measured using a Karl Fischer Titrator MA 101C (measuring range 10 ppm to 100% water contents). Mercury 4. 2. 0. Software was used for analyzing the crystal structure and intermolecular interactions.

General information

All reagents obtained commercially were utilized as received. NMR spectra were recorded using a 400 MHz NMR instrument, with chemical shifts (δ) expressed in parts per million (ppm) and spin–spin coupling constants (J) in Hertz (Hz). Multiplicities were designated as s (singlet), d (doublet), t (triplet), q (quartet), and m (multiplet). Tetramethylsilane (TMS) was used as the internal standard.

Theoretical calculations

The ground state (S_0) structure of optimization and vibrational frequency calculations of HCQ were performed using the DFT B3LYP/6-311+G(d,p) and CPCM method.[23–25] The calculated excited state transition energies were obtained using the TD DFT level using the same basis sets and functionals. All calculations were performed using the Gaussian 09[26,27] suite program. The output files were analyzed using Chemcraft software.

Synthesis

HCQ was prepared based on a previous literature report.[28]

DBU (10 mmol) was introduced into a solution of 2*H*-benzo[*d*]imidazole 1-oxide (10 mmol) and ethyl 2-cyanoacetate (10 mmol) in DMF (15 mL) at 0 °C. Initially, a violet color developed in the mixture, which was left to stir for an additional 10 minutes under the same conditions. After the consumption of the starting material as indicated by TLC, the reaction was quenched by adding 50 mL of cold-water containing conc. HCl (1 mL). The precipitate thus obtained was filtered and washed with CH_2Cl_2 (50 mL) to yield pure HCQ.

Compound HCQ was obtained as a bright yellow solid. Melting point: 234.3–235.7 °C. (85.5% yield). ^1H NMR (400 MHz, DMSO-d_6): δ (ppm): 12.48 (s, broad, 1H), 8.2 (dd, 1H, J = 8.6 Hz, J = 0.8 Hz), 7.93 (t, 1H, J = 7.8 Hz, J = 1.2 Hz), 7.83 (dd,1H, J = 8.6 Hz, J = 0.8 Hz), 7.51 (t, 1H, J = 7.8 Hz, J = 1.2 Hz).^{13}C NMR (101 MHz, DMSO-d_6): δ 152.0, 136.0, 134.4, 130.5, 125.2, 120.3, 118.4, 114.5, 111.9. HRMS: m/z $[M + H]^+$ Calculated: $C_9H_5N_3O_3$, 204.0409; found: 204.0387.

Results and discussion

Design of the probe and preliminary analysis

Our previous investigation showed variable responses of methyl and cyano substituents on the spectroscopic properties of cyanoquinoxaline *N*-oxide fluorophores[29] (Fig. 1). While AMQ was non-emissive, ACQ emitted at λ_{max} = 595 nm (577 nm in water). Based on the abovementioned study, it was envisaged that introducing a more electronegative heteroatom instead of nitrogen would enhance the acidity of the transferable hydrogen, thereby making the proton transfer process more feasible and possibly resulting in a considerable red shift in emission. The target molecule HCQ was initially synthesized, and subsequently, a detailed NMR analysis was carried out to understand the effect of solvent polarity on its structure.

In the ^{1}H NMR spectra in DMSO-d_6 and the D_2O:DMSO-d_6 mixture (2 : 3), an upfield shift of peaks was observed, indicating the structural modification of the compound/formation of a new ground state species (Fig. 2(a)). However, the peak positions and peak patterns remained the same in D_2O and CD_3OD, suggesting the prevalence of the same species in aqueous and methanolic environments (Fig. 2(b)). Introducing one equivalent of triethylamine (TEA) to the NMR sample in DMSO-d_6 revealed the generation of deprotonated species, plausibly existing in either enolate or keto form (Fig. 2(c)). However, the absence of a carbonyl peak in the ^{13}C NMR spectrum indicated the predominance of enolate species (Fig. 2(d)). The ^{13}C NMR spectra also showed an upfield shift for carbons at δ 136, 125.2, and 120.4 and a downfield shift for a peak at δ 114.5. In addition, a de-shielding of cyano carbon was observed with a shift in the δ value from 152 ppm to 154.8 ppm. The deshielding of cyano carbon plausibly arises due to the partial double bond character of the C–O$^-$ bond and its enhanced electron-withdrawing effect. Upon adding trifluoroacetic acid (TFA), a negligible influence on the ^{1}H and ^{13}C NMR spectrum was observed, confirming the existence of only enol form in DMSO in the absence/presence of acid.

Crystal data for HCQ were also recorded (CCDC 2270859†). It revealed a monoclinic crystal system, with the *C*2/*c* group having *a*, *b*, and *c* values of 16.4937 (3) Å, 8.07760 (10) Å, and 14.6807 (3) Å, respectively. We also carried out a detailed structural analysis of ACQ, whose crystal structure was already reported in our previous study (CCDC 2194801†).[29] A detailed structural analysis was necessary for this study to understand the effect of substituting nitrogen with oxygen in HCQ.

As shown by the crystal packing in ACQ (Fig. 3), the hydrogen bonds H3NA–N3 and H3NB–N3 both lie in the molecular plane and differ in bond length due to hydrogen bonding interaction with O1 and N4 of another molecule of ACQ (Fig. S34, ESI†). It was also validated by the dihedral angle values measured for N3–C5–C6–N1, O1–N2–C5–C6, O2–N1–C6–C5, and H3NB–N3–C5–C6 at −179.94°, −179.23°, 177.63° and −178.82° respectively (Table S11, ESI†) for ACQ. The dihedral angles for O1–N1–C9–C8 (178.43°), O3–N3–C8–C9 (−179.84°), and O2–C9–C8–N3 (178.64°) in HCQ also lie in a plane. However, in the same molecule, the measurements for H1–O1–N1–C9 (81.69°) and H1–O1–N1–C6 (−103.29°) confirm that the proton lies almost perpendicular to the plane and that the transfer of the proton takes place in the ground state. The elongated N1–O1 bond length of 1.3813 Å for HCQ further confirms the proton transfer because the typical O$^-$–N$^+$ bond is about 1.29 Å[28] as observed for O2–N1 (1.2792 Å), N2–O1 (1.3088 Å) for ACQ and O3–N3 (1.2638 Å) for HCQ. The length of the C9–O2 bond (1.2259 Å) lies between a C–O (∼1.45 Å) and a C=O (∼ 1.19 Å) bond, indicating that the C9–O2 bond attains a partial double bond character/bond length much closer to a carbonyl group (Table 1). The analysis shows the predominance of ground-state tautomerism in HCQ, in contrast to ACQ, which requires the presence of a base for the same. The observation in the case of HCQ is also substantiated by the observation from a previously reported *N*-oxide system with an ester substituent instead of –C≡N.[28] Besides, the crystal packing of HCQ also indicates the involvement of water molecules *via* hydrogen bonding and the concomitant proton transfer (Fig. S35, ESI†).

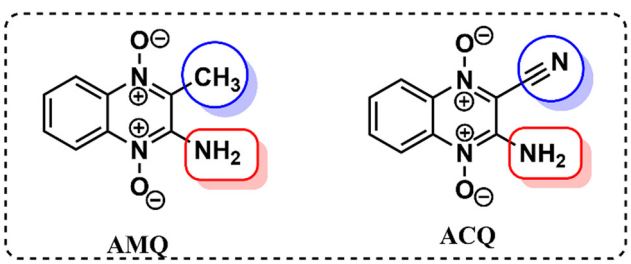

Fig. 1 Molecular structures of AMQ and ACQ.

Absorption, emission, and excitation spectra of HCQ

After thoroughly characterizing the probe, the basic photophysical properties of the system were explored. For a better understanding, solvatochromism data analysis was carried out by dividing the solvents into three categories: nonpolar (toluene, dioxane, THF, CH_2Cl_2), polar aprotic (CH_3CN, DMF, DMSO) and polar protic (MeOH, H_2O). The absorption spectra (Fig. 5(a)) of HCQ in different solvents indicate the possibility of the enol form (E), the deprotonated form (RO$^-$), and the keto form (K). Similarly, the fluorescence spectrum (Fig. 5(b)) indicates the possibility of three species, which could be the excited enol (E*), an excited deprotonated form (RO$^-$*), and the excited keto form (K*) (Fig. 4 and 6).

Toluene, dioxane, THF, and CH_2Cl_2. The absorbance spectra of HCQ in non-polar solvents show the predominance of one species (plausibly E) in its ground state, with an absorption peak at ∼410 nm. However, a minor shoulder peak was also observed at 520 nm in THF and dioxane. At an excitation wavelength of 420 nm, HCQ emits at ∼500 nm in all the non-polar solvents, indicating the prevalence of the E* form. This emission peak decreases upon increasing the excitation wavelength to > 480 nm, with a concomitant appearance of a low-intensity peak at ∼590–600 nm (possibly RO$^-$*/K*) (Fig. S2(c)–S2(5), ESI†). However, in the case of THF (Fig. S4(b), ESI†) and dioxane (Fig. S3(b), ESI†), more complex emission spectra were displayed with a gradual red shift in the emission maxima as the excitation wavelength was increased. Interestingly, the excitation spectra of HCQ in THF (Fig. S4(a), ESI†) and dioxane (Fig. S3(a), ESI†) showed only two peaks, with one peak at

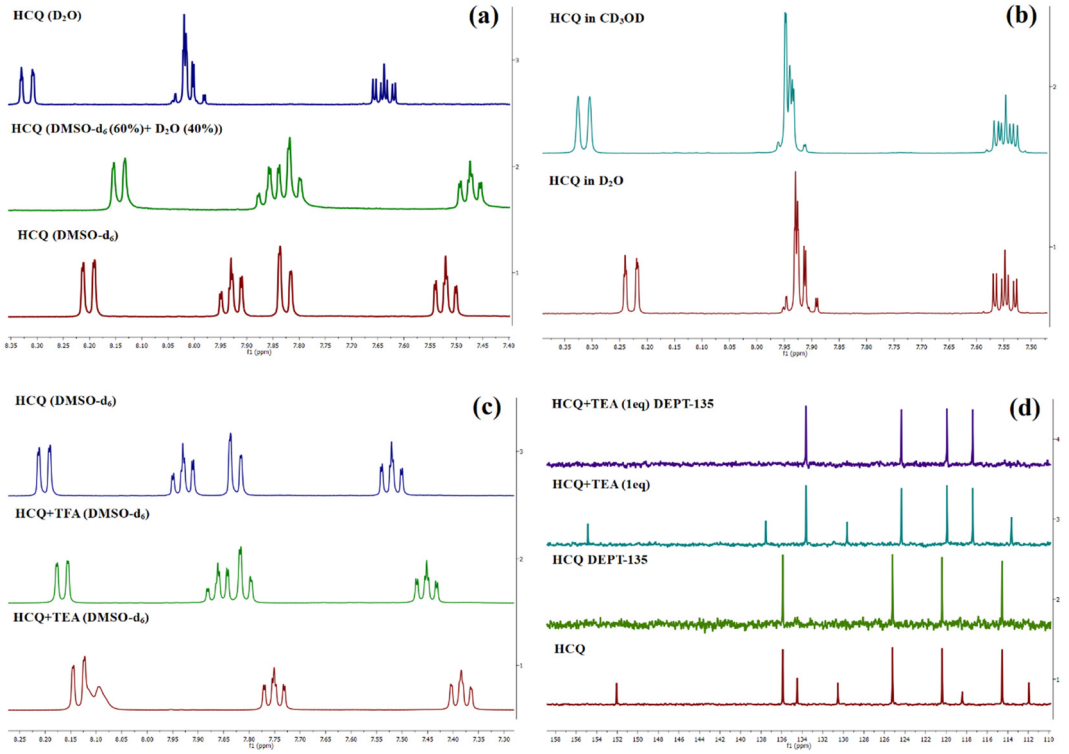

Fig. 2 (a)^{1}H NMR spectrum of HCQ in DMSO-d_6, D_2O, and DMSO-d_6 (60%) + D_2O (40%). (b) Comparison of similar splitting patterns in CD_3OD and D_2O. (c and d) Change in the ^{1}H and ^{13}C NMR spectrum of HCQ in the presence of triethyl amine (TEA) and trifluoroacetic acid (TFA).

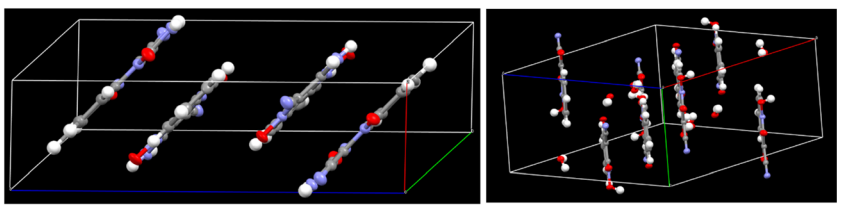

Fig. 3 Crystal packing in ACQ (left) and HCQ (right).

Table 1 Comparison of bond lengths for ACQ and HCQ

ACQ	Bond length (Å)	HCQ	Bond length (Å)
O2–N1	1.2792	O3–N3	1.2638
N1–C6	1.3558	N3–C8	1.3461
C6–C5	1.4203	C8–C9	1.4551
C5–N2	1.3525	N1–C9	1.3590
N2–O1	1.3088	N1–O1	1.3813
C5–N3	1.3294	C9–O2	1.2259
H3NA–N3	0.8200	O1–H1	0.8401
H3NB–N3	0.8752		

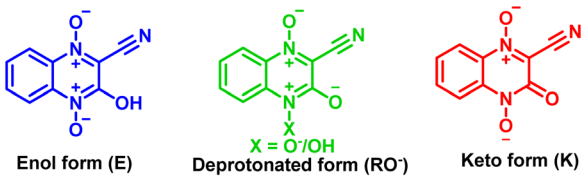

Fig. 4 Possible forms of HCQ in solution.

~410 nm and another at ~500 nm. In toluene (Fig. S2(a), ESI†) and CH_2Cl_2 (Fig. S5(a), ESI†), the picture was much simpler due to a substantial overlap of both the absorbance and excitation spectra, thus showing the predominance of the E form in the ground state. The existence of two species (plausibly E and E*) is very evident for toluene and CH_2Cl_2 from the absorbance, excitation, and emission spectra (Fig. S2(b) and S5(b), ESI†), while the complex emission spectra observed in the case of THF and dioxane are difficult to explain at this juncture and will require further investigations.

CH_3CN, DMF, and DMSO. As per literature reports, CH_3CN, DMSO, and DMF have a certain basicity, and acids tend to dissociate in these solvents.[31–33] The donor numbers (DN) of these solvents follow the order CH_3CN < DMF < DMSO.

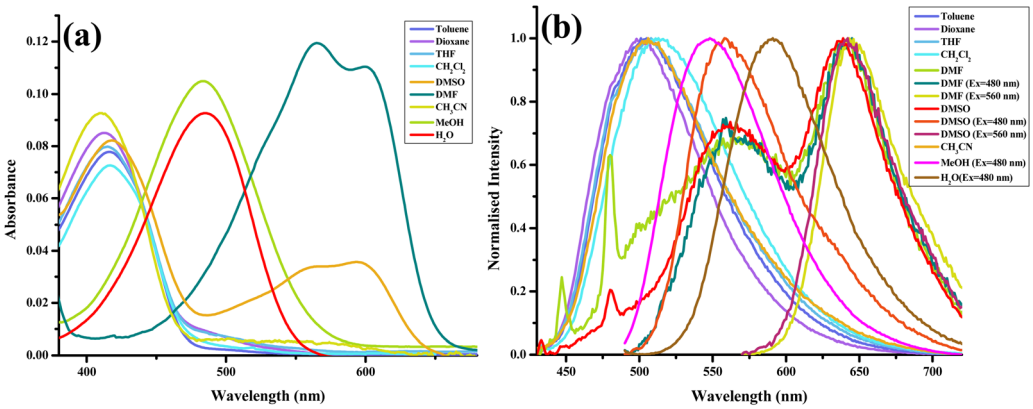

Fig. 5 (a) Absorption spectra. (b) Normalised emission (λ_{ex} = 420 nm) spectra of HCQ (10 μM) in solvents of varying polarities (note: arranged according to E_T (30) with toluene-lowest to water-highest).[30]

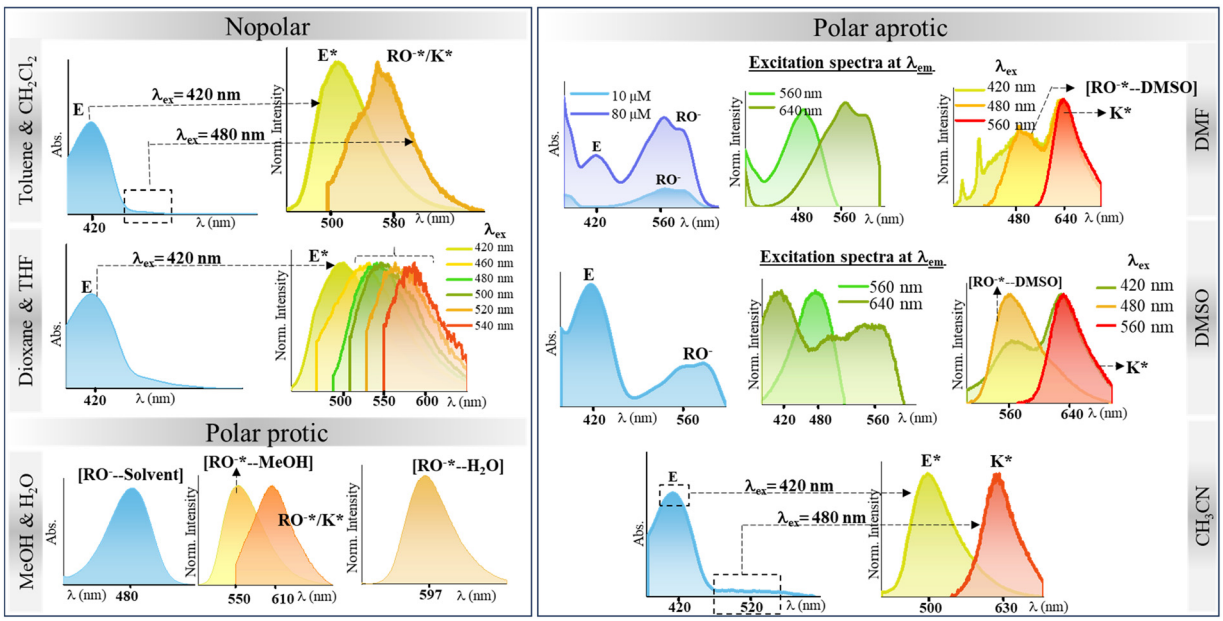

Fig. 6 Overview of spectral responses of HCQ in solvents of varying polarities.

For HCQ, the position of its absorption spectrum varied depending on the solvent, with a more significant red shift in λ_{max} for DMF and DMSO compared to CH_3CN. In both DMSO and DMF, the absorption spectra of HCQ exhibited a broad peak at 560 nm, with an additional peak at ~410 nm in DMSO. The availability of non-bonded electrons in DMSO and DMF makes them basic in nature and facilitates hydrogen transfer in the ground state *via* the GSIPT/GSPT route. This plausibly leads to the dissociation of HCQ and the emergence of a shoulder at 560 nm in the absorption spectra. The 410 nm band in DMSO resembles a similar peak observed in nonpolar solvents, which can be attributed to the E form. In DMF, a variable absorbance behavior was observed with a change in the HCQ concentration (Fig. S6(d), ESI†). While the 560 nm band persisted at 10 μM, the appearance of the 410 nm band was noticed when the concentration was increased beyond 40 μM. Increasing HCQ concentration in DMSO leads to the saturation in absorbance signal at 560 nm, possibly due to limited solvent availability with respect to the probe concentration (Fig. S7(d), ESI†). According to us, it prevents further deprotonation of HCQ molecules by the solvent. In CH_3CN, the 530 nm peak is subdued due to the solvent's low DN. Upon excitation at 420 nm, emission spectra reveal two peaks, possibly E* and RO^-*/K*. In CH_3CN, HCQ exhibits a peak at 500 nm and an additional band at 630 nm, observed only when the excitation was >480 nm (Fig. S8(b), ESI†). Excited state investigations conducted in DMSO, DMF, and CH_3CN reveal the presence of two distinct species. In acetonitrile, excitation spectra (Fig. S8(a), ESI†) recorded at emission wavelengths beyond 560 nm showed the emergence of a peak at 530 nm. This occurrence may be ascribed to the prevalence of only the K* form within the wavelength range of ~500–540 nm and RO^-*/

K* beyond 540 nm. Interestingly, excitation spectra monitored at varying λ_{em} in DMSO and DMF failed to show any peak at ~410 nm for λ_{em} 560 nm; instead, a peak around 480 nm was observed, which was not observed in the absorbance spectra. The maximum fluorescence intensity was also achieved at an excitation wavelength of 480 nm for both solvents (Fig. S6(c) and S7(c), ESI†). In both DMF and DMSO, the 640 nm peak was more pronounced than the 560 nm peak at lower excitation (410 nm). A similar observation was also reported by Das *et al.*[34] HCQ exhibited dual emission, with a distinct blue band centered around ~560 nm and ~640 nm in DMF and DMSO. The intensity of the 560 nm peak in DMSO increased with an excitation wavelength of 480 nm but gradually diminished with a further increase in excitation wavelength beyond 500 nm. The emergence of a 640 nm peak started beyond λ_{ex} = 500 nm. Notably, the intensity ratio between both emitting species varied with the excitation wavelength, as depicted in the λ_{ex} plots (Fig. S6(b)–S7(b), ESI†). This indicated that the dual emission was linked to the excitation wavelength, and the concentration of the two species depended on the excitation energy. The origin of the 560 nm absorption band in DMF and DMSO could be from the RO^- anion of the ground state. On the other hand, the emission band seen at ~560 nm could be due to a solvated hydrogen-bonded complex in the excited state.[34] Furthermore, the experimental absorbance and emission of HCQ were compared to the results of TD DFT/B3LYP/6-311+G(d,p), and their corresponding oscillator strengths in CH_3CN using a CPCM model are tabulated in Table S12 (ESI†). The experimental absorbance and emission values of enol and keto forms were in agreement with the theoretically predicted peak positions, further confirming that the ~410 nm absorbance and ~500 nm emission bands correspond to the enol form and the ~520 nm absorbance and ~630 nm emission bands can be assigned to the keto form [Fig. S37 and S39, ESI†].

MeOH and water. In MeOH and water, the absorption maxima at 480 nm correspond to the deprotonated form (RO^-/RO^-—solvent). This conclusion relied on the preliminary NMR analysis in D_2O/CD_3OD (Fig. 2(b)) and XRD data. MeOH and water, being polar protic solvents, show the same spectral features in the ground state, which indicates the existence of a single species (plausibly RO^-/T). However, the excited state features in both solvents vary drastically. Two species were observed in methanol at 550 and 610 nm (Fig. S9(b), ESI†). On the other hand, in water, only one form at 597 nm was observed (Fig. S10(b), ESI†), even with varying excitation wavelengths. However, the excitation spectra in methanol and water showed a single peak at different λ_{em}, similar to its absorption spectra (Fig. S9(a) and S10(a), ESI†).

Spectral features of the protonated and deprotonated forms

To gain further insights into the ground state and excited state forms in diverse solvents, solvatochromism (Fig. 7(a) and 8(a)) and solvatofluorochromism (Fig. 7(b) and 8(b)) of HCQ were studied under acidic (trifluoroacetic acid, TFA) and basic (triethylamine, TEA) conditions. In the presence of 100 μM TFA, in all solvents, the UV-visible spectrum showed a peak at ~410 nm, initially observed only in non-polar solvents. This observation indicated that all the deprotonated/solvated forms can be converted to the E form in the presence of acid. Interestingly, for THF and dioxane, where a complex emission spectrum was initially observed, the presence of acid revealed a peak at ~500 nm, which did not show any shift upon changing the excitation wavelength. Even the excitation spectrum overlapped with the absorbance spectrum of all solvents, demonstrating the prevalence of only one form in the ground state in an acidic environment. Noticeably, acid addition did not impact the emission wavelength of DMSO, DMF, MeOH, and water. The origin of such behavior could be the higher excited state acidity of the probe, which allows the proton to be transferred to either the acceptor N^+–O^- group/solvent in the presence of a high energy excitation wavelength of 420 nm.

In the presence of TEA (100 μM), the disappearance of the peak at ~410 nm and the concomitant increase in the absorption peak between 530 and 580 nm were observed for most solvents. This observation confirms that the 530–580 nm band in the absorbance spectrum of HCQ in DMSO, DMF, and CH_3CN arises due to the deprotonation and that the E form and the RO^-/K form exist in equilibrium in the ground state. However, no change in the absorbance signal was observed in water and MeOH. Similarly, in the excited state, the red-shifted emission band ranging from 578–643 nm appears at

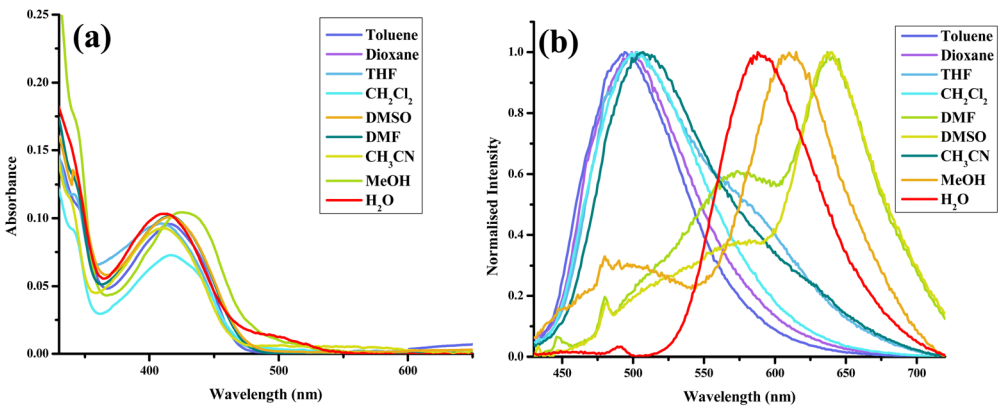

Fig. 7 (a) Absorbance and (b) normalised emission spectra (λ_{ex} = 420 nm) of HCQ (10 μM) with TFA (100 μM) in solvents of varying polarities.

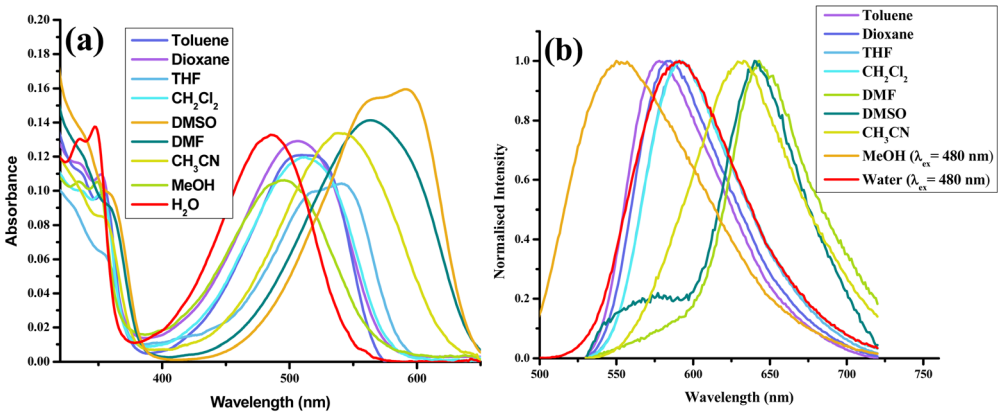

Fig. 8 (a) Absorbance and (b) normalised emission spectra (λ_{ex} = 520 nm) of HCQ (10 μM) with TEA (100 μM) in solvents of varying polarities. (Note: λ_{ex} for MeOH and water was kept at 480 nm since no changes in response to base were observed in the UV spectrum.)

λ_{ex} = 520 nm except for MeOH and water, where the emission spectrum remains unaltered in the presence of a base.

This study helped us to establish the prevalence of an enol E form and a deprotonated (RO^-)/keto (K) form in the ground state of HCQ.

Fluorescence decay of HCQ

On completion of the preliminary photophysical studies, we focused on a detailed analysis of the lifetime for HCQ at different emission wavelengths. Fluorescence quantum yields (ϕ_F) and lifetimes (τ) were measured, followed by radiative (k_r) and non-radiative rate constants (k_{nr}). These data, along with steady-state fluorescence information, are summarized in (Table S1, ESI†).

Our initial study measured lifetimes at the blue and red end maxima of the emission spectra (Tables S2, S3 and Fig. S22, S23, ESI†). In addition, the obtained data were also compared with the lifetimes of the protonated and deprotonated species. The lifetime of the pure deprotonated form was obtained using a lower energy excitation laser source (510 nm) as it eliminates the interferences from all the species that emit below this excitation. It gave only one lifetime indicative of its keto/deprotonated state (Table S4 and Fig. S24, ESI†). For the protonated form, a certain percentage of the tautomeric isomer also persisted (Table S5 and Fig. S25, ESI†).

As observed in the fluorescence spectra of dioxane-HCQ and THF-HCQ conjugates, emission varied with excitation wavelength, which indicated the presence of multiple spectral components. In toluene and CH_2Cl_2, only two species/components were observed. At ~500 nm, the lifetimes observed in these four solvents lie in the range of ~0.45–0.55 ns. The lifetime obtained at red-end emission maxima for these solvents was inconsistent, possibly due to the HCQ–solvent interactions. However, upon deprotonation, the lifetimes were obtained in the ~2.2–2.6 ns range.

Based on a large Stokes shift, the emission peak at $\lambda_{em} \approx$ 630–643 nm in CH_3CN, DMSO, and DMF under basic conditions was attributed to the emission from RO^-*/K* forms. This observation is comparable to the lifetime data (~1.4–1.6 ns) obtained at the same wavelength for the solvent–HCQ ensemble without any acidic/basic additive. Additionally, the minor component observed only in DMSO-HCQ and DMF-HCQ combinations ranging from ~1.4–1.6 ns showed an overall small amplitude (<11.7%). This indicated the presence of a small percentage of tautomeric form even at 560 nm and the prevalence of this species at 640 nm as a major component, as shown by the similar lifetime range. Apart from the E* and RO^-*/K* forms, other components with lifetimes > 9 ns also exist in DMSO and DMF, plausibly arising due to the solvent–probe interactions. However, even upon protonation in DMF and DMSO, the persistence of a longer lifetime component of HCQ obtained at ~640 nm was in line with the keto/deprotonated form. This observation shows the significant impact of proton transfer in an excited state. Interestingly, CH_3CN, despite being a polar aprotic solvent, showed an intermediate behavior between nonpolar and polar aprotic solvents since the protonated form lifetime of ~0.4 ns (>88.36%) lies close to that in non-polar solvents while the deprotonated state lifetime lies in the range of ~1.4–1.6 ns which is similar to that in DMF and DMSO (Fig. 10).

Overall monitoring of lifetimes at the blue end of the spectrum with their emission at ~500 nm in toluene, dioxane, THF, CH_2Cl_2, and CH_3CN and ~560 nm in DMSO and DMF also confirms the presence of two different species in these solvents. The scatter plot for solvents depicts that at ~500 nm, the major component has a lifetime of ~0.4 ns and ~0.2 ns at ~560 nm. While the red end spectrum (~640 nm) lifetime of species generated in CH_3CN, DMF, and DMSO is ~1.4–1.6 ns and ~2.4–2.6 ns at 570–590 nm in toluene, dioxane, THF, and CH_2Cl_2 which corresponds to the RO^-*/K* form (Fig. 9).

In water, the decay profile of HCQ exhibited a single exponential fit, indicating the prevalence of a single species irrespective of protonation or deprotonation at 597 nm. In MeOH, the decay lifetime revealed a tri-exponential decay at 610 nm, with a major component showing a lifetime of ~0.84 ns. This value is comparable to that of water (~0.7 ns), suggesting that the solvent environment in MeOH influences the excited state dynamics in a way that resembles that of water. Under acidic conditions, both MeOH–HCQ and water–HCQ conjugates exhibit

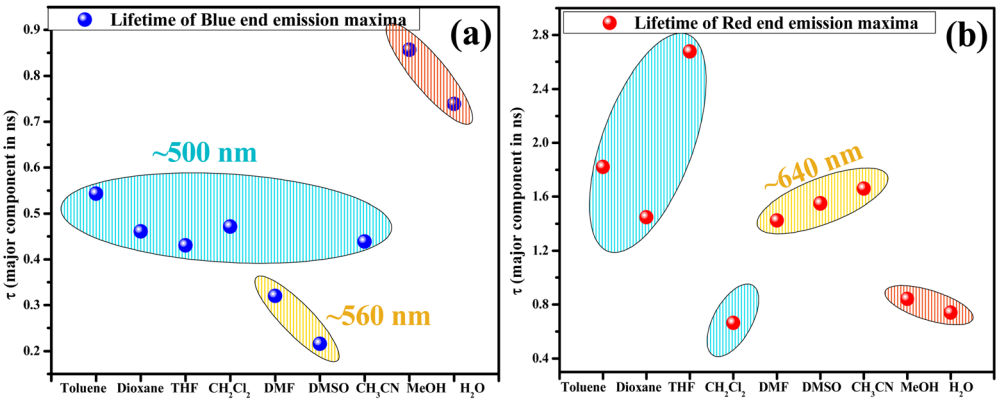

Fig. 9 Scatter plot depicting the lifetime (ns) of the major component at respective λ_{em} in a pure solvent monitored at (a) blue end and (b) red end of the emission spectrum.

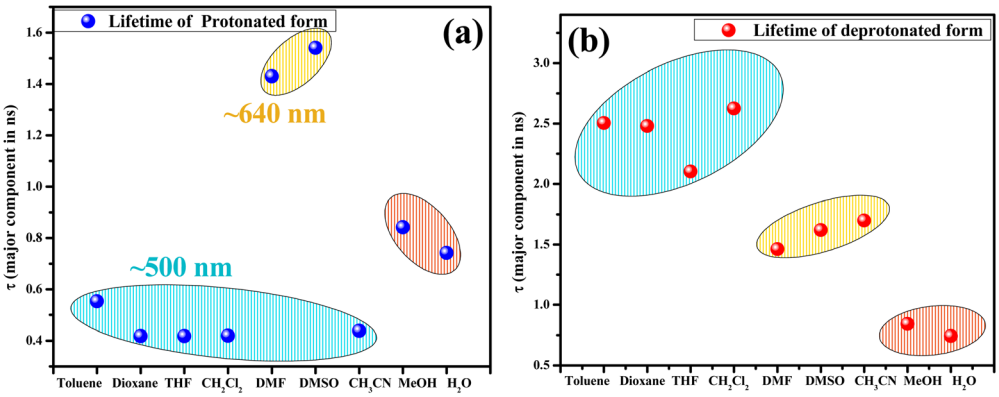

Fig. 10 Scatter plot depicting the lifetime (ns) of the major component at respective λ_{em} for (a) the protonated and (b) the deprotonated form. [Note: In DMSO and DMF, the lifetime corresponding to λ_{em} 640 nm are shown for the protonated form because the maximum intensity was obtained at 640 nm. The 560 nm lifetimes are tabulated in Table S3, ESI†].

a mono-exponential decay with comparable lifetimes. Shorter lifetimes in protic solvents at longer emission wavelengths can be attributed to the participation of the solvent molecules in the proton transfer process and the likely involvement of the ESIPT/ESPT mechanism.14 In order to substantiate the role of water molecules in the *N*-oxide proton transfer site, TD DFT B3LYP/6-311+G(d,p) calculations with excited state optimization of the [RO^-—H_2O] complex using a CPCM model in water were carried out. The oscillator strengths are tabulated in Table S12 (ESI†). The correlation between observed and predicted absorbance (505 nm) and emission spectra (599 nm) further substantiates a possible interaction between HCQ and water molecules [Fig. S39, ESI†].

Water detection

We decided to explore HCQ's potential for water detection by relying on its unique/stable photophysical response in the polar protic solvents against other solvents (Fig. 11). Despite the availability of traditional analytical techniques for assessing water content in organic solvents, there is a growing need to develop easily implementable methods for routine laboratory tasks and industrial applications.[35] Various fluorescent probes are known for detecting trace water levels in organic solvents, from probes relying on mechanisms such as aggregation-induced emission/aggregation-caused quenching[36–38] and hydrogen bonding to anti-Kasha emission.[39,40]

Our initial attempt started with dioxane and THF (Fig. S26–S29, ESI†). Herein, the addition of water in varying amounts in the dioxane–HCQ and THF–HCQ solution led to a decrease in the intensity of the absorption peaks at 412 nm and 415 nm, respectively, and a concomitant increase in the peaks at 500 nm and 519 nm, respectively. Due to the formation of multiple species in the excited state in dioxane and THF, these solutions were initially treated with 100 μM TFA before starting the fluorescence titration. It was done to generate a single system that can respond effectively to the variable water concentration. In the case of CH_3CN, an inconsistent response was observed in the ground state signals upon titration with water (Fig. S31, ESI†). This forced us to conduct water analysis only *via* the fluorescence method by treatment with 100 μM TFA. Results included in the ESI for dioxane, THF, and acetonitrile reveal a consistent trend as the water content increased from 0–3%. The fluorescence intensity dropped at ~500 nm, accompanied by a

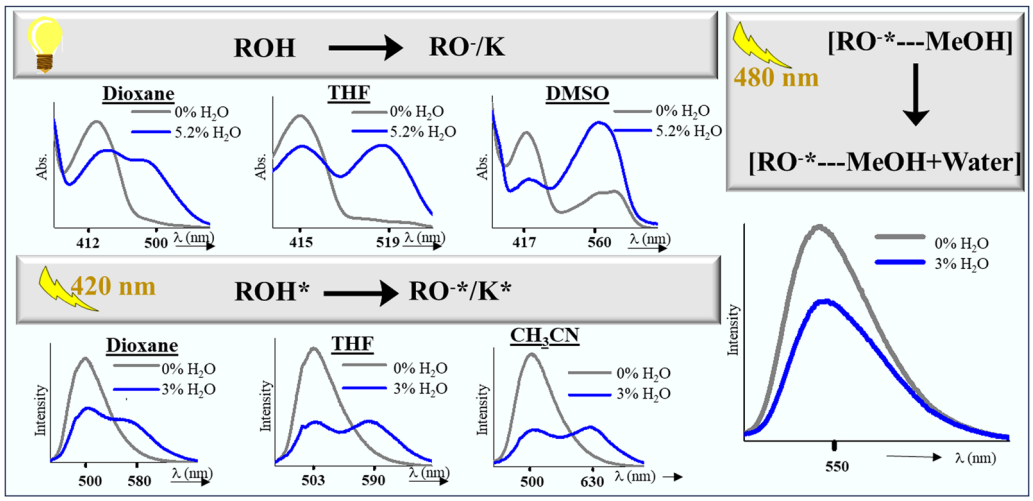

Fig. 11 Overview of water detection using HCQ in different solvents.

gradual red-shift in emission peak and an increase at 580 nm, 590 nm, and 630 nm, respectively. This variation in the turn-on fluorescence response stems from the solvent's variable polarities and solvation abilities. The limit of detection/quantitation (LOD/LOQ) of water for these solvents ranged from 0.001–0.08% and 0.09–0.9%, respectively (Table 2). Similar experiments with DMSO did not furnish any spectral responses towards water in the excited state; however, in the ground state, the peak at 412 nm decreased in intensity with a simultaneous increase in the intensity at 560 nm (Fig. S30, ESI†). Due to the prevalence of the deprotonated form in the ground state and inconsistent responses in the ground and excited state, water detection could not be carried out in DMF. In methanol, the water content was determined using the fluorescence route, where a decrease in the peak intensity at λ_{max} 550 nm was observed, with a gradual increase in the water concentration (Fig. S32(a), ESI†). After completing the preliminary experiments, unknown samples were analyzed using the developed method. Volunteers were asked to prepare these samples in dry solvents with variable percentages of water (<3%) for further analysis. These samples were then recorded using fluorescence and UV spectrometers, and the value of the ratio of wavelengths as specified for each solvent was matched with the tabulated percentage range from the titration plot. To ensure the accuracy and reliability of the water content analysis, the same samples were also screened using a Karl Fischer titrator, further validating the obtained results (Tables S6–S10, ESI†).

The mechanism of detection

Two factors are mainly responsible for detecting water in the abovementioned solvents. In the solvents dioxane, THF, CH_3CN, and DMSO that showed a bathochromic shift *via* absorption/fluorescence, the basis of water detection was an interplay of various excited state structures of HCQ. Water detection in methanol, on the other hand, relied on a hypochromic shift in peak intensity at λ_{em} = 550 nm (Fig. 11).

Water detection *via* absorbance in dioxane, THF, and DMSO was possible due to the difference in their absorption maxima compared to water. Although observed even in CH_3CN, this difference was only significant beyond a 10% water concentration (Fig. S33, ESI†). The absence of pronounced spectral changes in CH_3CN can be attributed to its linear molecular structure, which allows the formation of a tighter solvent shell around the HCQ molecule, unlike dioxane, THF, and DMSO.

The detection of water in the dioxane–HCQ, THF–HCQ, and CH_3CN–HCQ ensembles using the fluorescence technique relied on the previous analysis of the protonated states. In the presence of an acid, a single-emitting species was observed at λ_{em} = 500 nm, corresponding to the enol form as confirmed earlier. Due to the prevalence of a certain percentage of the keto

Table 2 Summary of water detection of HCQ in various organic solvents

Solvent	Detection method	Shift in λ	LOD (%)	LOQ (%)	R^2	Standard error[a] (±)	Water content (%)
Dioxane	Absorbance	Bathochromic	0.0483	0.4724	0.9972	0.0016	0–5.2
	Fluorescence	Bathochromic	0.0864	0.9204	0.9964	0.0030	0–3
THF	Absorbance	Bathochromic	0.0238	0.2588	0.9673	0.0072	0–5.2
	Fluorescence	Bathochromic	0.0265	0.1773	0.9290	0.0226	0–3
CH_3CN	Fluorescence	Bathochromic	0.0522	0.3576	0.9423	0.0158	0–3
DMSO	Absorbance	Bathochromic	0.0015	0.0942	0.9871	0.0089	0–5.2
MeOH	Fluorescence	Hypochromic	0.2854	1.7093	0.9962	0.0020	0–3

[Note: For dioxane, THF, and CH_3CN, 100 μM TFA was used along with HCQ only for fluorescence titration.] [a] Standard error denoted is from the slope of the calibration curve for three repeated experiments.

form in these solvents at higher excitation, TFA was utilized to completely shift the equilibrium to the enol form (only for fluorescence titration in dioxane, THF, and CH_3CN). Based on this, the excitation at 420 nm of the protonated form yielded emission peaks between 580 and 630 nm, which could be used to observe the effect of titration with water. Mechanistically, it is the water-assisted shifting of the equilibrium to the enolate/keto form.

The water detection method in methanol differs from that observed in other solvents. Although the ground state behavior of HCQ in methanol and water is comparable, the emission spectra differ by a wavelength of 47 nm (550 nm in MeOH and 597 nm in water). This disparity enabled water detection in methanol in the excited state using a λ_{ex} of 480 nm.

Conclusion

The proton transfer capability of cyanoquinoxaline-*N*-oxide fluorophore HCQ has been demonstrated in this work. A detailed static/dynamic photophysical study of the probe in solvents of varying polarities, along with studies under acidic/basic conditions, disclosed the propensity of the probe to exist in variable structural entities. Owing to its stable behavior in the aqueous environment, the probe was also explored for detecting water in common organic solvents. It displayed advantages such as high sensitivity and rapid response. Given the simplicity of the probe structure, further efforts are undertaken in our laboratory to improve its sensitivity.

Author contributions

Savita: conceptualisation, methodology, investigation, and writing – original draft. Adarash Kumar Shukla: methodology, investigation, and discussion. Anupam Bhattacharya: conceptualisation, resources, supervision, funding acquisition, and writing – review and editing.

Data availability

Supporting data pertaining to this article have been included in the ESI.†

Conflicts of interest

The authors declare that they have no known competing financial interests or personal relationships that could have appeared to influence the work reported in this paper.

Acknowledgements

BITS-Pilani is acknowledged for the CDRF research grant (C1/23/138) and the Department of Science and Technology, Government of India, for the FIST grant (SR/FST/CS-I/2020/158). We thank Prof. Srikanta Dinda and Mr Apalla Reddy from the Department of Chemical Engineering, BITS-Pilani Hyderabad Campus, for providing access to the Karl Fischer instrument and for valuable discussions.

References

1 D. Ghosh, S. Batuta, S. Das, N. A. Begum and D. Mandal, Proton Transfer Dynamics of 4′-N,N-Dimethylamino-3-hydroxyflavone Observed in Hydrogen-Bonding Solvents and Aqueous Micelles, *J. Phys. Chem. B*, 2015, **119**(17), 5650–5661.
2 S. Youssif, Recent trends in the chemistry of pyridine N-oxides, *ARKIVOC*, 2001, **1**, 242–268.
3 J. d Klerk, I. H. van Stokkum, A. Szemik-Hojniak, I. Deperasinska, C. Gooijer, H. Zhang, W.-J. Buma and F. Ariese, Excited state processes of 2-butylamino-6-methyl-4-nitropyridine N-oxide in nonpolar solvents. A transient absorption spectroscopy study, *J. Phys. Chem. A*, 2010, **114**(12), 4045–4050.
4 S. Leyva-Ramos and A. Pedraza-Alvarez, Quinoxaline 1, 4-di-N-oxides: a review of the importance of their structure in the development of drugs against infectious diseases and cancer, *Med. Chem. Res.*, 2021, **30**(6), 1175–1184.
5 J. M. Turner and A. J. Messenger, Occurrence, biochemistry and physiology of phenazine pigment production, *Adv. Microb. Physiol.*, 1986, **27**, 211–275.
6 X. Shen and K. S. Gates, Enzyme-activated generation of reactive oxygen species from heterocyclic N-oxides under aerobic and anaerobic conditions and its relevance to hypoxia-selective prodrugs, *Chem. Res. Toxicol.*, 2019, **32**(3), 348–361.
7 G. Cheng, W. Sa, C. Cao, L. Guo, H. Hao, Z. Liu, X. Wang and Z. Yuan, Quinoxaline 1, 4-di-N-oxides: biological activities and mechanisms of actions, *Front. Pharmacol.*, 2016, **7**, 64.
8 Z. Ma, J. Li, K. Lin, M. Ramachandran, M. Li and Y. Li, Heterocyclic N-Oxides as Small-Molecule Fluorogenic Scaffolds: Rational Design and Applications of Their ''On–Off'' Fluorescence, *Anal. Chem.*, 2020, **92**(18), 12282–12289.
9 A. Shukla, V. T. N. Mai, V. V. Divya, C. H. Suresh, M. Paul, V. Karunakaran, S. K. M. McGregor, I. Allison, K. N. Narayanan Unni, A. Ajayaghosh, E. B. Namdas and S.-C. Lo, Amplified Spontaneous Emission from Zwitterionic Excited-State Intramolecular Proton Transfer, *J. Am. Chem. Soc.*, 2022, **144**(30), 13499–13510.
10 B. Poór, N. Michniewicz, M. Kállay, W. J. Buma, M. Kubinyi, A. Szemik-Hojniak, I. Deperasińska, A. Puszko and H. Zhang, Femtosecond Studies of Charge-Transfer Mediated Proton Transfer in 2-Butylamino-6-methyl-4-nitropyridine N-Oxide, *J. Phys. Chem. A*, 2006, **110**(22), 7086–7091.
11 A. Szemik-Hojniak, I. Deperasińska, L. Jerzykiewicz, P. Sobota, M. Hojniak, A. Puszko, N. Haraszkiewicz, G. van der Zwan and P. Jacques, Crystal Structure, Spectroscopic, and Theoretical Investigations of Excited-State Proton Transfer in the Doubly Hydrogen-Bonded Dimer of 2-Butylamino-6-methyl-4-nitropyridine N-Oxide, *J. Phys. Chem. A*, 2006, **110**(37), 10690–10698.

12 J. S. de Klerk, A. Szemik-Hojniak, F. Ariese and C. Gooijer, Intramolecular Proton-Transfer Processes Starting at Higher Excited States: A Fluorescence Study on 2-Butylamino-6-methyl-4-nitropyridine N-Oxide in Nonpolar Solutions, *J. Phys. Chem. A*, 2007, **111**(26), 5828–5832.

13 J. d Klerk, I. H. M. van Stokkum, A. Szemik-Hojniak, I. Deperasińska, C. Gooijer, H. Zhang, W.-J. Buma and F. Ariese, Excited State Processes of 2-Butylamino-6-methyl-4-nitropyridine N-oxide in Nonpolar Solvents. A Transient Absorption Spectroscopy Study, *J. Phys. Chem. A*, 2010, **114**(12), 4045–4050.

14 A. Szemik-Hojniak, Ł. Wiśniewski, I. Deperasińska, A. Makarewicz, L. Jerzykiewicz, A. Puszko, Y. Erez and D. Huppert, The impact of solvent polarity on intramolecular proton and electron transfer in 2-alkylamino-4-nitro-5-methyl pyridine N-oxides, *Phys. Chem. Chem. Phys.*, 2012, **14**(22), 8147–8159.

15 A. P. Demchenko, V. I. Tomin and P.-T. Chou, Breaking the Kasha Rule for More Efficient Photochemistry, *Chem. Rev.*, 2017, **117**(21), 13353–13381.

16 N. A. Shekhovtsov, E. B. Nikolaenkova, A. S. Berezin, V. F. Plyusnin, K. A. Vinogradova, D. Y. Naumov, N. V. Pervukhina, A. Y. Tikhonov and M. B. Bushuev, A 1-Hydroxy-1H-imidazole ESIPT Emitter Demonstrating anti-Kasha Fluorescence and Direct Excitation of a Tautomeric Form, *ChemPlusChem*, 2021, **86**(10), 1436–1441.

17 N. A. Shekhovtsov, K. A. Vinogradova, S. N. Vorobyova, A. S. Berezin, V. F. Plyusnin, D. Y. Naumov, N. V. Pervukhina, E. B. Nikolaenkova, A. Y. Tikhonov and M. B. Bushuev, N-Hydroxy–N-oxide photoinduced tautomerization and excitation wavelength dependent luminescence of ESIPT-capable zinc(ii) complexes with a rationally designed 1-hydroxy-2,4-di(pyridin-2-yl)-1H-imidazole ESIPT-ligand, *Dalton Trans.*, 2022, **51**(25), 9818–9835.

18 N. A. Shekhovtsov, A. A. Ryadun and M. B. Bushuev, Luminescence of a Zinc (II) Complex with a Protonated 1-Hydroxy-1H-imidazole ESIPT Ligand: Direct Excitation of a Tautomeric Form, *ChemistrySelect*, 2021, **6**(44), 12346–12350.

19 N. A. Shekhovtsov, E. B. Nikolaenkova, A. S. Berezin, V. F. Plyusnin, K. A. Vinogradova, D. Y. Naumov, N. V. Pervukhina, A. Y. Tikhonov and M. B. Bushuev, Tuning ESIPT-coupled luminescence by expanding π-conjugation of a proton acceptor moiety in ESIPT-capable zinc (II) complexes with 1-hydroxy-1 H-imidazole-based ligands, *Dalton Trans.*, 2022, **51**(39), 15166–15188.

20 N. A. Shekhovtsov, E. B. Nikolaenkova, S. N. Vorobyova, V. F. Plyusnin, K. A. Vinogradova, T. S. Sukhikh, A. Y. Tikhonov and M. B. Bushuev, Luminescence of ESIPT-capable zinc (II) complexes with a 1-hydroxy-1 H-imidazole-based ligand: exploring the impact of substitution in the proton-donating moiety, *Dalton Trans.*, 2023, **52**(23), 8114–8134.

21 N. A. Shekhovtsov, E. B. Nikolaenkova, A. A. Ryadun, D. G. Samsonenko, A. Y. Tikhonov and M. B. Bushuev, ESIPT-Capable 4-(2-Hydroxyphenyl)-2-(Pyridin-2-yl)-1 H-Imidazoles with Single and Double Proton Transfer: Synthesis, Selective Reduction of the Imidazolic OH Group and Luminescence, *Molecules*, 2023, **28**(4), 1793.

22 L. M. Carneiro, A. F. Keppler, F. F. Ferreira, P. Homem-de-Mello and F. H. Bartoloni, Mechanisms for the Deactivation of the Electronic Excited States of α-(2-Hydroxyphenyl)-N-phenylnitrone: From Intramolecular Proton and Charge Transfer to Structure Twisting and Aggregation, *J. Phys. Chem. B*, 2022, **126**(38), 7373–7384.

23 M. Cossi, V. Barone, R. Cammi and J. Tomasi, Ab initio study of solvated molecules: a new implementation of the polarizable continuum model, *Chem. Phys. Lett.*, 1996, **255**(4–6), 327–335.

24 M. Cossi, N. Rega, G. Scalmani and V. Barone, Energies, structures, and electronic properties of molecules in solution with the C-PCM solvation model, *J. Comput. Chem.*, 2003, **24**(6), 669–681.

25 M. Cossi and V. Barone, Time-dependent density functional theory for molecules in liquid solutions, *J. Chem. Phys.*, 2001, **115**(10), 4708–4717.

26 M. Frisch; F. Clemente, M. J. Frisch, G. W. Trucks, H. B. Schlegel, G. E. Scuseria, M. A. Robb, J. R. Cheeseman, G. Scalmani, V. Barone, B. Mennucci, G. A. Petersson, H. Nakatsuji, M. Caricato, X. Li, H. P. Hratchian, A. F. Izmaylov, J. Bloino and G. Zhe, *Gaussian 09, revision a. 01*, 2009, 20–44.

27 M. J. Frisch, G. W. Trucks, H. B. Schlegel, G. E. Scuseria, M. A. Robb, J. R. Cheeseman, G. Scalmani, V. Barone, G. A. Petersson, H. Nakatsuji, *et al.*, *Gaussian09, R., 01*, Gaussian Inc., Wallington, CT, 2016.

28 Y. Xu, F. Wu, Z. Yao and M. Z. S. Jiang, Synthesis of quinoxaline 1, 4-di-N-oxide analogues and crystal structure of 2-carbomethoxy-3-hydroxyquinoxaline-di-N-oxide, *Molecules*, 2011, **16**(8), 6894–6901.

29 C. Savita, A. Nandikolla, A. K. Shukla, K. V. G. Chandra Sekhar and A. Bhattacharya, Visible light sensing of ions by a cyanoquinoxaline 1,4-dioxide-based probe and its applications, *Dalton Trans.*, 2023, **52**(13), 4103–4111.

30 J. P. Cerón-Carrasco, D. Jacquemin, C. Laurence, A. Planchat, C. Reichardt and K. Sraïdi, Solvent polarity scales: determination of new ET(30) values for 84 organic solvents, *J. Phys. Org. Chem.*, 2014, **27**(6), 512–518.

31 I. Kolthoff and T. Reddy, Acid-base strength in dimethyl sulfoxide, *Inorg. Chem.*, 1962, **1**(2), 189–194.

32 I. M. Kolthoff, M. K. Chantooni and H. Smagowski, Acid-base strength in N, N-dimethylformamide, *Anal. Chem.*, 1970, **42**(13), 1622–1628.

33 A. Kütt, S. Tshepelevitsh, J. Saame, M. Lõkov, I. Kaljurand, S. Selberg and I. Leito, Strengths of acids in acetonitrile, *Eur. J. Org. Chem.*, 2021, (9), 1407–1419.

34 R. Das, S. Mitra and S. Mukherjee, Proton transfer and anion formation in the ground and excited states of 4-methyl-2, 6-diformyl phenol in highly polar aprotic solvents, *J. Photochem. Photobiol., A*, 1993, **76**(1–2), 33–38.

35 R. Oguchi, K. Yamaguchi and T. Shibamoto, Determination of Water Content in Common Organic Solvents by a Gas Chromatograph Equipped with a Megabore Fused-Silica Column and a Thermal Conductivity Detector, *J. Chromatogr. Sci.*, 1988, **26**(11), 588–590.

36 H. S. Jung, P. Verwilst, W. Y. Kim and J. S. Kim, Fluorescent and colorimetric sensors for the detection of humidity or water content, *Chem. Soc. Rev.*, 2016, **45**(5), 1242–1256.
37 F. Wu, L. Wang, H. Tang and D. Cao, Excited State Intramolecular Proton Transfer Plus Aggregation-Induced Emission-Based Diketopyrrolopyrrole Luminogen: Photophysical Properties and Simultaneously Discriminative Detection of Trace Water in Three Organic Solvents, *Anal. Chem.*, 2019, **91**(8), 5261–5269.
38 C. Zhang, X. Li, Z. Li, Y. Wang, J. Lu, L. Zhu and F. Zhang, Two-Stage Three-Dimensional Luminescent Sensing Strategy for Precisely Detecting a Wide Range of Water Content in Tetrahydrofuran, *Anal. Chem.*, 2022, **94**(19), 7004–7011.
39 H. Sun, S.-S. Sun, F.-F. Han, Y. Zhao, M.-D. Li, B.-X. Miao, J. Nie, R. Zhang and Z.-H. Ni, Water-stimuli-responsive dynamic fluorescent switch from Kasha's rule to anti-Kasha's rule based on a tetraphenylethene substituted Schiff base, *Chem. Eng. J.*, 2021, **405**, 127000.
40 Y. Zhou, G. Baryshnikov, X. Li, M. Zhu, H. Ågren and L. Zhu, Anti-Kasha's Rule Emissive Switching Induced by Intermolecular H-Bonding, *Chem. Mater.*, 2018, **30**(21), 8008–8016.

